Performance simulations for the ground-based, expanded-beam x-ray source BEaTriX

Spiga, Daniele, Salmaso, Bianca, Basso, Stefano, Ghigo, Mauro, Sironi, Giorgia, et al.

Daniele Spiga, Bianca Salmaso, Stefano Basso, Mauro Ghigo, Giorgia Sironi, Gabriele Vecchi, Vincenzo Cotroneo, Paolo Conconi, Giovanni Pareschi, Gianpiero Tagliaferri, Marcos Bavdaz, Ivo Ferreira, Luigina Arcangeli, Massimilano Rossi, Vadim Burwitz, Surangkhana Rukdee, Gisela Hartner, Thomas Mueller, Thomas Schmidt, Andreas Langmeier, Desiree Della Monica Ferreira, Nis C. Gellert, Sonny Massahi, Finn E. Christensen, "Performance simulations for the ground-based, expanded-beam x-ray source BEaTriX," Proc. SPIE 11837, Advances in X-Ray/EUV Optics and Components XVI, 118370O (21 September 2021); doi: 10.1117/12.2595033

SPIE.

Event: SPIE Optical Engineering + Applications, 2021, San Diego, California, United States

Performance simulations for the ground-based, expanded-beam X-ray source BEaTriX

D. Spiga*, B. Salmaso, S. Basso, M. Ghigo, G. Sironi, G. Vecchi,
V. Cotroneo, P. Conconi, G. Pareschi, G. Tagliaferri
INAF-Osservatorio Astronomico di Brera, Via E. Bianchi 46, 23807 Merate (Italy)

M. Bavdaz, I. Ferreira
European Space Agency, Keplerlaan 1, 2201 AZ Noordwijk (Netherlands)

L. Arcangeli, M. Rossi
Media Lario Srl, via al Pascolo, 23842 Bosisio Parini (Italy)

V. Burwitz, S. Rukdee, G. Hartner, T. Müller, T. Schmidt, A. Langmeier
Max-Planck-Institüt für extraterrestrische Physik, Garching (Germany)

D. Della Monica Ferreira, N. C. Gellert, S. Massahi, F. E. Christensen
DTU-space, Juliane Maries Vej 30, DK-2100 Copenhagen (Denmark)

ABSTRACT

The BEaTriX (Beam Expander Testing X-ray) facility, being assembled at INAF-Brera Astronomical Observatory, will represent an important step in the acceptance roadmap of Silicon Pore Optics (SPO) mirror modules, and so ensure the final angular resolution of the ATHENA X-ray telescope. A paraboloidal mirror, manufactured at INAF-Brera, will provide a collimated X-ray beam to a monochromating system and to a beam expansion unit, enabling the full illumination of the mirror modules under test with a broad, highly monochromatic, and parallel X-ray beam. Such a beam will be used to directly diagnose SPO modules in their focusing performances. This requires, indeed, the expanded beam to have a divergence smaller than the expected angular resolution of the modules under test. This condition is subject, in turn, to the optical quality and to the alignment of the optical components. Aiming at establishing the final angular resolution that can be reached and the respective fabrication/positioning tolerances, we have been dealing with a comprehensive set of optical simulations. Modeling based on wave optics and ray-tracing was carried out to predict the collimation performances of the paraboloidal mirror, including the effect of surface errors obtained from metrology. Ray-tracing routines were subsequently employed to simulate the full beamline. This paper reports the simulation results and the methodologies we have adopted.

Keywords: BEaTriX, X-ray test facility, collimating mirror, optical simulations, wave optics, ray-tracing

1. INTRODUCTION

On-ground test and calibration of imaging optics for X-ray telescopes have always posed a problem. First, they require large vacuum systems to accommodate optical systems that have become increasingly large over time. Secondly, the large focal lengths at play not only require a long range in vacuum; the oncoming beam has to be highly collimated (e.g., nearly parallel) to simulate the incidence from a source at virtually infinite distance. Since X-rays are hardly handled by means of refractive systems, this requirement entails locating the source at very large distance - like PANTER at MPE,[1] or the XRCF beamline at MSFC - with a further increase in the vacuum volume and the pumping-down time. Even though these two facilities represent worldwide reference points in the calibration of astronomical X-ray optics, they are hardly adoptable to perform the individual tests of the more than 600 elements that will compose the imaging module of the ATHENA X-ray telescope.[2]

* corresponding author: daniele.spiga@inaf.it, phone +39-0272320-427

Advances in X-Ray/EUV Optics and Components XVI, edited by Christian Morawe
Ali M. Khounsary, Shunji Goto, Proc. of SPIE Vol. 11837, 118370O · © 2021 SPIE
CCC code: 0277-786X/21/$21 · doi: 10.1117/12.2595033

The ATHENA (Advanced Telescope for High-ENergy Astrophysics) X-ray telescope is the second large mission selected by ESA within the Cosmic Vision Program, with launch scheduled in the early 2030s. It will be the largest X-ray telescope ever built, with a 2.5 m diameter, a 1.4 m^2 effective area at 1 keV, and an angular resolution of 5 arcsec half-energy width (HEW). Such a large focusing system cannot be manufactured with monolithic mirrors; it will be populated with modular elements, termed as MMs (*mirror modules*), based on *silicon pore optics* (SPO), a technology conceived and developed by ESA and the *Cosine* company (Warmond, The Netherlands), where SPO MMs will be manufactured in series.[3] After manufacturing, however, the focusing properties of MMs need to be qualified through a measurement of their *point spread function* (PSF) and *effective area* (EA). Currently, tests of SPO MMs are performed at the XPBF 2.0 beamline of the BESSY II light source.[4] Nevertheless, the beam at BESSY is too small to enable a full illumination of the MM aperture in a single shot, and the characterization is achieved by scanning the optical element and reconstructing the PSF.[5] Full aperture measurements of SPO MMs have been performed at PANTER[6] to validate the qualification process ongoing at BESSY. Despites, a routinely and systematic qualification of the mirror modules coming from the production pipeline, at a foreseen rate of 2-3 MMs/day, demands a dedicated facility with reduced vacuum-venting cycles and able to generate a parallel and wide X-ray beam.

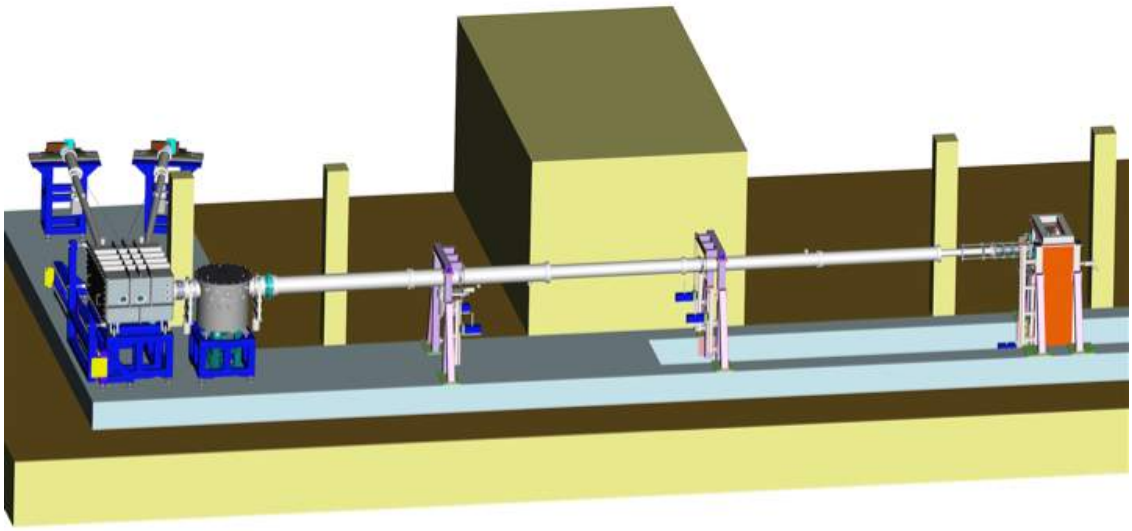

Figure 1: final layout of the BEaTriX facility (Tecnomotive design). The two short arms foreseen for the two X-ray energies (4.51 keV and 1.49 keV) are visible on the left side of the picture. The squared optical chamber houses the optical elements that filter, collimate, and expand the beam to a 17 cm × 6 cm size. The cylindrical chamber will enclose the MM to be tested, whose focus will be inspected right at the end of the long arm (left to right in the picture). All the components are under vacuum (10^{-6} mbar).

These motivations urged us to design and develop the BEaTriX (*Beam Expander Testing X-ray facility*) system[7] with the specific purpose of performing the functional tests of SPO modules prior to their integration into the mirror assembly of ATHENA. Following a number of updates over years,[8][9][10] BEaTriX has been finalized (Figure 1) in its design[11] and, owing to a number of grants (ESA, AHEAD, ASI, INAF), it is now in advanced status of completion at INAF-Brera, Merate.[12] BEaTriX will generate a 17 cm × 6 cm parallel (≈ 2 arcsec) beam at either 1.49 keV or 4.51 keV. The beam will probe the SPO MMs that will be delivered from the production site, generating its X-ray focal spot on a CCD camera at a 12 m distance, and enabling the selection of the most performing modules to be aligned optically and integrated into the mirror assembly at the nearby company Media Lario.[13] The final mirror assembly of ATHENA will be ready for test and calibration at the VERT-X facility,[14] to be built next to the integration bench.

In this paper, we show the methodologies and the results of the simulations performed to assist the manufacturing of the optical components, with particular reference to the paraboloidal mirror, and so determine the expected performances of the final beam in terms of collimation, intensity, and uniformity. We briefly introduce the optical elements of BEaTriX in Sect. 2, even though a detailed description of the complete system can be found in another SPIE volume.[15] In Sect. 3, we provide a description of the metrological tools used to measure the paraboloidal mirror, the methods adopted for simulating its performance, and those of the entire system. In Sect. 4, we compare the mirror simulations with the experiment at PANTER. In Sect. 5, we describe the expanded beam we expect from metrology data. Sect. 6 provides a brief update on the wavefront sensing technique that will be used to align the paraboloidal mirror to the X-ray source.

2. THE BEATRIX X-RAY FACILITY

BEaTriX is a vacuum system consisting of two arms (Figure 1), approximately forming a right angle, fitting within a small lab (17 m × 8 m). The short arm generates, collimates, filters and expands the X-ray beam that will illuminate the SPO MM to be tested; the long arm enables the propagation of the focused beam over a 12 m range, out to the focal plane. The short arm will comprise two beamlines, one at 1.49 keV (the Al- Kα1 line) and another at 4.51 keV (the Ti- Kα1 line), while the long arm is in common for the two energies. To date, we have almost completed the 4.51 keV beamline, while the realization of the 1.49 keV beamline is envisaged to start soon.

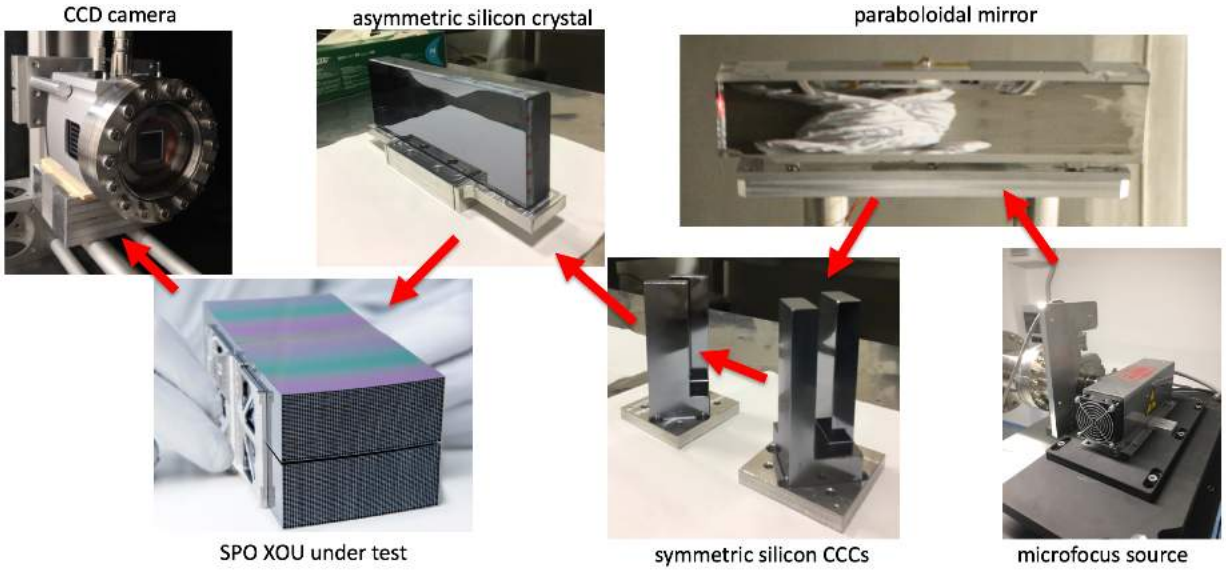

Figure 2: schematic of the optical chain in BEaTriX. X-rays are generated by an X-ray source with titanium anode (by Incoatec GmbH, Geesthacht, Germany) that uniformly illuminates a mirror in the shape of a paraboloid. The beam, now made parallel and expanded vertically to a 60 mm size, is spectrally filtered by a 4-bounce silicon monochromator (a pair of channel-cut crystals by Crystal Scientific Ltd, UK) to isolate a narrow portion of the Ti-Kα line. The monochromatic beam impinges onto the asymmetric crystal (by IMEM-CNR, Parma, Italy), which diffracts the beam at a nearly-right angle, expanding it horizontally to a 17 cm width. The beam then illuminates the aperture of an SPO MM or XOU, which forms its PSF on a CCD (provided by Andor Techn. Ltd.). Auxiliary components (vacuum pumps/gauges, beam monitors, slits, vacuum motors…) are not shown in this paper.

In the 4.51 keV beamline (Figure 2), the X-ray beam is generated by a microfocus source (a gaussian with 35 μm FWHM) with titanium anode, pre-collimated by a 400 μm diam. pinhole at a 2 cm distance. The source is located in the focus of a paraboloidal mirror at a 4.75 m distance, at the other end of the short arm, which makes the beam parallel and 6 cm tall. This paraboloid, pre-shaped by Zeiss, has been accurately polished and figured at INAF-Brera,[16] and coated at DTU with a 30 nm platinum layer to endow the mirror with reflection properties at 4.51 keV. A 4 nm chromium layer was deposited underneath the platinum to improve the coating adhesion. The following steps enable the horizontal expansion of the X-ray beam, exploiting the principle of diffraction by an asymmetrically-cut crystal.[17] Due to the dispersivity of asymmetric crystals,[18] however, the beam has to be made tightly monochromatic by a couple of channel cut crystals, mutually de-tuned in angle to narrow the spectral bandpass down to 30-50 meV.[19] The monochromatic beam is expanded horizontally to a 17 cm dimension by an asymmetric-cut silicon crystal, making it ready to illuminate the aperture of a MM. The focused beam is collected by a CCD, 12 m farther. In the 1.49 keV beamline, silicon crystals will have to be replaced by organic crystals (ADP),[20] which will require a separate setup.

All the optical components are enclosed in a system of vacuum tubes and chambers able to reach 10^{-6} mbar. The vacuum sections are partitioned by gate valves, in order to drastically abridge the time required for breaking and making the vacuum in the chamber that will house the MM. The long arm can be tilted to fit the reflection angle of the MM. All the components can be moved by precise vacuum motors and the entire system is controlled by dedicated software based on LabVIEW. The entire facility is built on building foundations to ensure its stability, and mounted on a heavy and damped anti-vibration platform made of reinforced concrete (Figure 3). More details on the configuration of the BEaTriX system can be found in a dedicated paper.[15]

Figure 3: the status of the BEaTriX lab in May 2020 (left) and in July 2021 (right). All the vacuum system was realized and installed by Kenosistec (Binasco, Italy) in a building basement and mounted on an anti-vibration platform. The chambers enclose the optical components that will expand and parallelize the X-ray beam. All the system fits within 17 m × 8 m.

3. MIRROR METROLOGY AND SIMULATION TOOLS

3.1. The mirror metrology tools (MPR and CCI)

The heart of the system is the paraboloidal mirror. The vertical divergence of the final beam essentially depends on the X-ray source size and is affected only by the transverse deviations of rays, which always have a lesser magnitude due to the incidence at a grazing angle. In contrast, the optical quality of the mirror is crucial in determining the horizontal collimation, the intensity, and the uniformity of the expanded beam. For this reason, a relevant effort has been devoted to polish and figure the paraboloid. The two tools used at INAF-Brera for taking the mirror within the prescribed specification are shown in Figure 4 and the finishing process are duly described in another contribution.[21] After every polishing or figuring iteration, the shape and the roughness of the mirror were accurately measured using the metrological tools available at Media Lario. This gave us feedback for the next iterations and allowed us simulating the expected performances of the expanded beam at every step of the surface working.

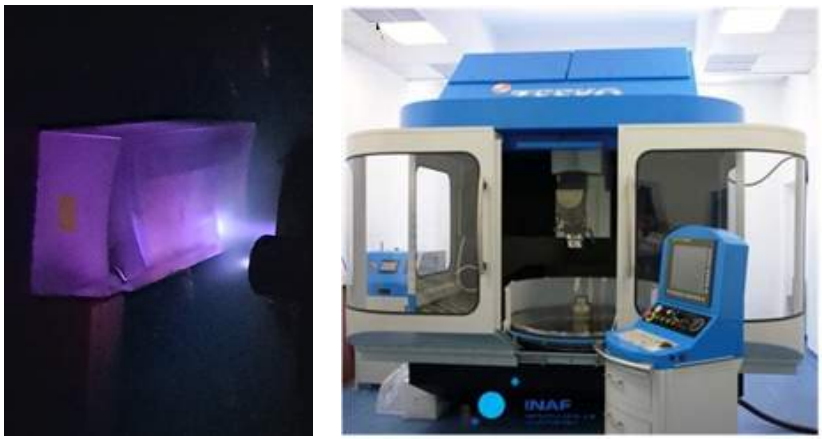

Figure 4: two steps in the manufacturing of the paraboloidal mirror at INAF-Brera. Left: Ion Beam Figuring for figure correction. Right: Zeeko IRP1200 polishing machine for roughness mitigation.

The metrology tools are the Mandrel Profilometer-Rotondimeter (MPR) and the CCI micro-interferometer, both operated at Media-Lario. MPR is a contactless and versatile shape detector,[22] developed in collaboration with LT Ultra Precision Technology GmbH. For measuring the BEaTriX mirror, an appropriate interface has been designed, and dedicated routines have been developed to reliably extract the error map, filtering the instrument dynamics out. The mirror has been characterized in the central 400 mm × 60 mm area (Figure 5, left), which fully encloses the beam involved in the asymmetric diffraction, at a 1 mm lateral resolution and a single-point vertical resolution of a few

nanometers. CCI is a phase shift interferometer coupled to microscopes with magnifications 2.5×, 10×, 50×, developed by Taylor-Hobson. It returns 2D maps of the mirror surface microtopography, enabling assessment of the surface roughness. A 10× image of a surface's sampled point, in its final polishing state, is displayed in Figure 5, right. For both shape and roughness measurements, we note that residual defects and polishing marks have the same orientation as the optical axis; this minimizes their impact on the beam divergence in the horizontal plane. At the same time, owing to the incidence at a grazing angle of $\alpha = 0.91$ deg, ray deviations in the vertical plane are damped by a factor of $\tan\alpha = 0.0157$. In principle, only in-plane scattering could have been modeled from the longitudinal power spectral density, using the well-experienced 1D formalism.[23] Indeed, the marked anisotropy of roughness could make the out-of-plane scattering non-negligible, so we opted for a scattering modeling method in 2D (see next section).

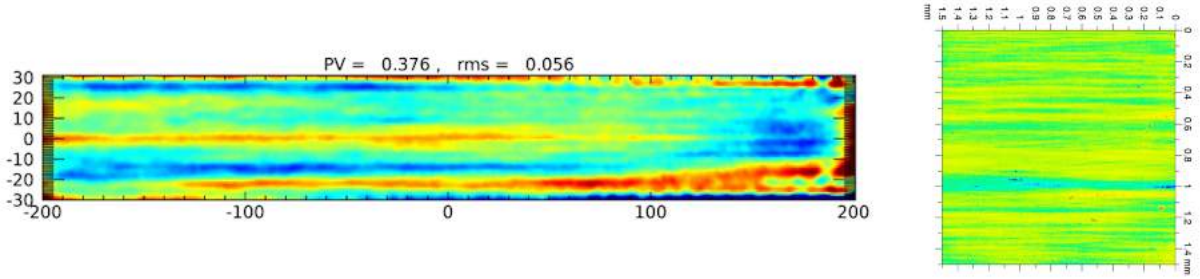

Figure 5: two typical metrological outputs for the BEaTriX paraboloidal mirror. Left: profile error map of the central 400 mm × 60 mm area of the collimating mirror surface, in its final manufacturing status, as obtained from the MPR at Media Lario; the optical axis is horizontal, vertical units are in microns. Right: a 10× image sampled on the mirror by the CCI micro-interferometer operated at Media Lario, RMS x: 5.1 Å, RMS y: 3.5 Å. The optical axis is aligned horizontally.

3.2. The BEaTriX mirror simulation

Two different codes were used for modeling the focus of the BEaTriX mirror. One is a conventional ray-tracing routine, taking as input the MPR map and the 2D scattering model derived from the CCI maps. A 2D scattering pattern is used to pseudo-randomly generate the in-plane and out-of-plane deviation angles, β and γ. We defer to Appendix A details about the inclusion of both deviation angles into a ray-tracing routine.

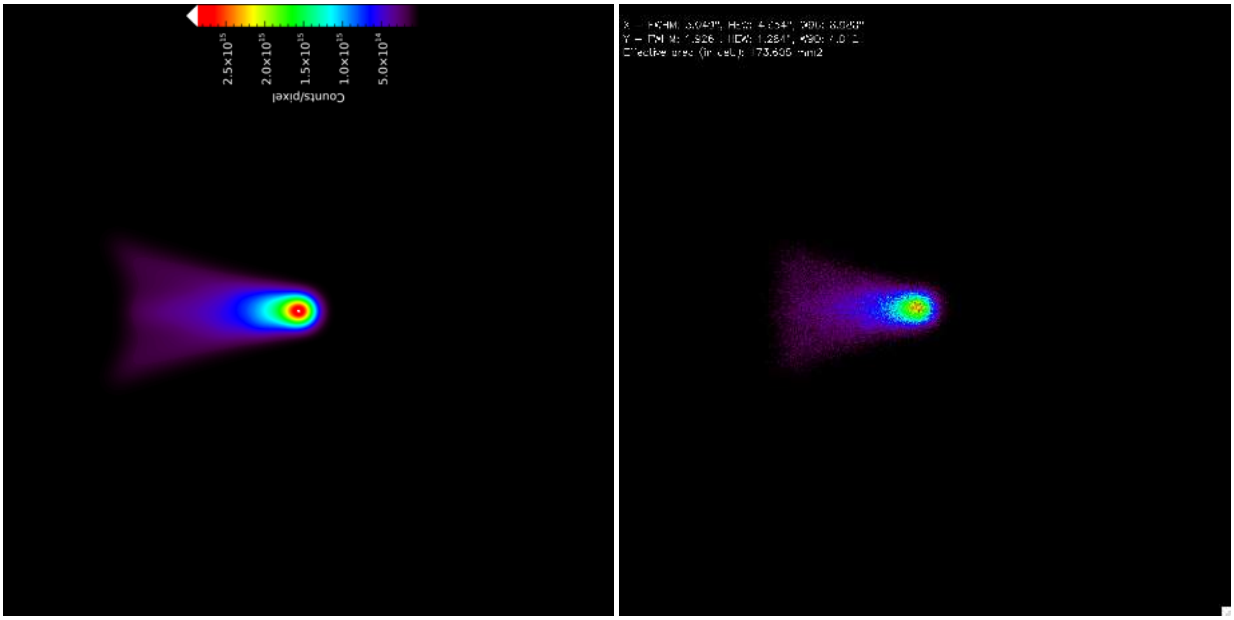

Figure 6: the simulated focal spot of the perfect paraboloid *in diverging X-ray illumination at PANTER. The best focus is located 200 mm farther from the source, with respect to the nominal focal distance. Even there, a small coma aberration remains, so a correction of the incident wavefront using a zone plate is necessary. The mirror faces the left side. Left: diffraction pattern at 1.49 keV from wavefront propagation. Right: result of a ray-tracing routine. The image sizes are 2 mm.*

The other simulation code computes the diffraction pattern from the OPD (optical path differences) introduced by mirror defects, misalignments, and the measurement setup, such as an X-ray source at a finite distance. For this code, we have used the same approach adopted in the SIMPOSIuM project to simulate silicon pore optics,[24] and in the VERT-X project to determine the alignment tolerances between the two segments of the Wolter-I collimator.[25] For instance, we show in Figure 6, left, the expected aberration at PANTER due to the very large, but finite, distance D of the X-ray source from the mirror aperture, at the nominal incidence angle α, even after re-adjusting the detector plane to the shifted best focus. The related OPD term is:

$$\Delta l_{\mathrm{D}} = \frac{x^2 + y^2}{2D} + \frac{(x^2 + y^2)x}{4D^2 \tan\alpha \sin\alpha} \tag{1}$$

where x and y are the aperture pupil coordinates, with the origin in the mirror aperture center and the mirror facing left. The first term is the spherical aberration, easily corrected moving the focal plane at a distance f' fulfilling the relation $1/f' = 1/f - 1/D$. The second term generates the coma aberration, which can be removed only making the incident beam parallel; at PANTER, this can be done at 1.49 keV by means of a zone plate[26] as collimating optic. The expectations from the diffraction code and the ray-tracing code (Figure 6, right) exactly match each other.

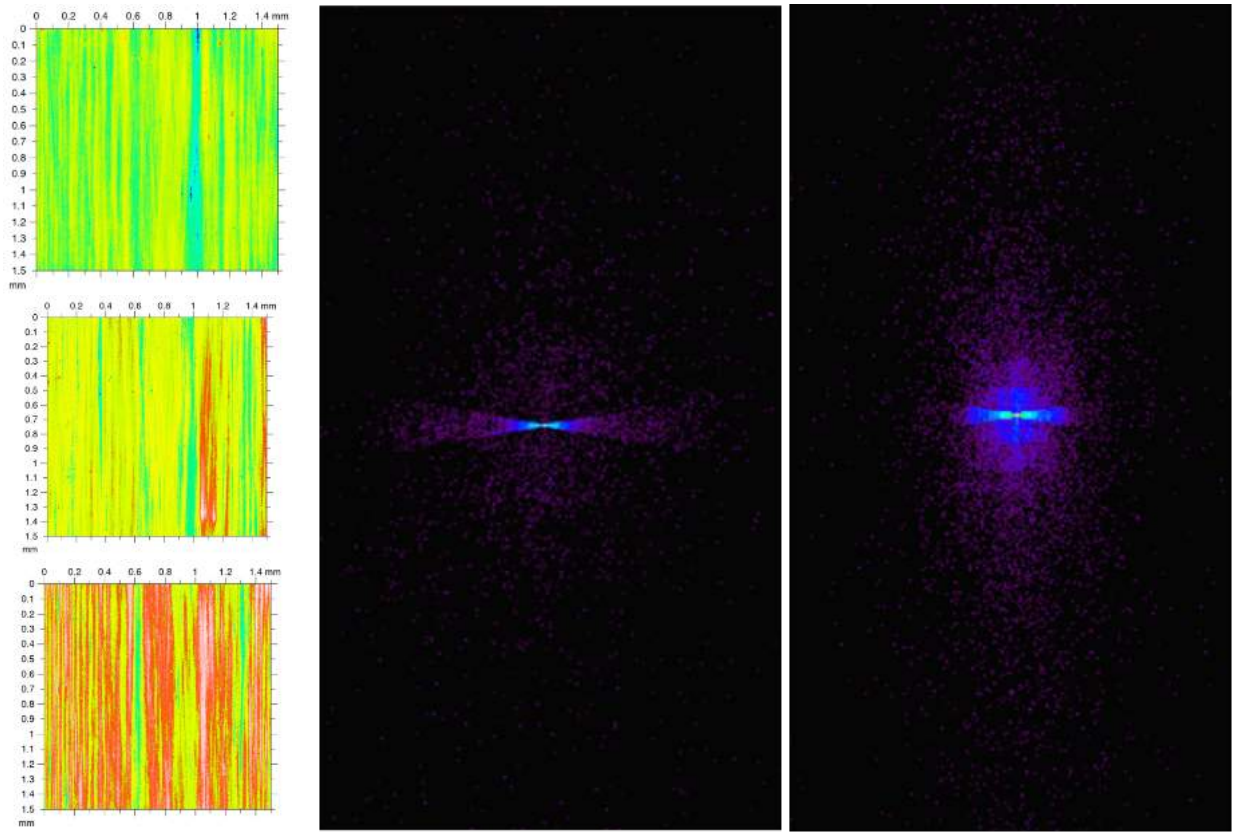

Figure 7: simulated diffraction pattern from mirror roughness. Left: a number of microtopography images taken on the BEaTriX mirror with CCI 10× have been stitched along the optical axis (in vertical) in order to obtain a 2D scattering diagram via the FFT of the complex pupil function (CPF). Center: expected diffraction pattern at 1.49 keV, HEW < 0.2 arcsec. Right: expected diffraction pattern at 4.51 keV, HEW < 0.5 arcsec. The color scale is logarithmic. The image widths are 18 arcsec.

As for the scattering component, the marked anisotropy of the roughness pattern requires computing the scattering distribution in 2D, directly using the 10× CCI microtopography maps as diffractive objects, projected along the line of sight, and taking the squared module of the Fourier transform of the phase shift map CPF.[24] Because the axial direction y is seen in projection in grazing incidence, a number of CCI maps were stitched together in a column to avoid contribution from aperture diffraction (along x, it is negligible as it is). The expected diffraction patterns at 1.49 keV and 4.51 keV are shown in Figure 7: as a consequence of the roughness directionality, even at a shallow angle incidence, X-ray scattering is preferentially *orthogonal* to the incidence plane. Anyway, at both energies, the scattering contribution to the HEW remains very small.

3.3. The BEaTriX full simulation code

Besides the simulation of the mirror alone, it is important to understand whether the finishing of the mirror surface is sufficient to guarantee the collimation, uniformity, and intensity properties of the expanded beam. We have thereby used the full BEaTriX simulation program (Figure 8), already developed and used to define the fabrication and the alignment tolerances of the entire system.[19] The following input data have been used:

- A source radiance of 10^{11} ph/s/sterad (in the Kα doublet) from a Ti-anode source of 35 μm FWHM;
- X-ray absorption in the residual atmosphere (10^{-6} mbar);
- reflectivity of the Pt-coated paraboloidal mirror at 0.9 deg incidence;
- paraboloidal mirror metrology (shape error + 2D scattering);
- reflectivity of a Si (220) double CCC, with a relative 12 arcsec rotation in order to narrow the energy passing band to 0.05 eV;[15]
- reflectivity and dispersivity of a Si (220) crystal cut at an asymmetry angle of 44.592 deg;
- all the possible misalignments between components.

We so obtain as output the expected vertical and horizontal divergence, dimensions, intensity, and uniformity of the expanded beam. Optionally, one can also simulate an SPO MM module that focuses the expanded beam.

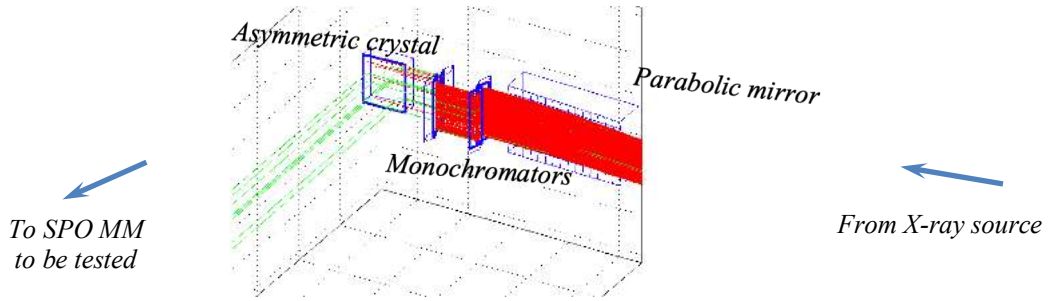

Figure 8: a simple graphical rendition of the BEaTriX simulation code. The rays from the X-ray source are pre-selected by a slit properly shaped to filter only the rays that will finally strike upon the asymmetric crystal. Red rays are absorbed by some optical element. Eventually, green rays populate the expanded beam.

In order to get statistically significant results, 10^7 rays need to be launched at least. This means that, to keep the computation time within reasonable limits, rays cannot be traced at small steps as usual. Rays are traced from their origin in the source to the intersection with each optical element, in a single "big leap", computing the intersection point analytically. This is very easy in the case of crystals, because their surfaces are planar. Given the position of a ray $\underline{r}_0$ and its direction $\underline{k}_0$ before reflection (where $|\underline{k}_0| = 1$), the ray is represented by the equation:

$$\vec{r}_1(t) = \vec{r}_0 + t\vec{k}_0 \tag{2}$$

where t is a positive parameter expressing the distance of $\underline{r}_1$ from $\underline{r}_0$. The equation of a reflecting planar face π with normal $\underline{n}_\pi$, independent of the impact point, and passing by a point $\underline{r}_c$ (e.g., the face center) is

$$(\vec{r}_1 - \vec{r}_c) \cdot \vec{n}_\pi = 0. \tag{3}$$

By substitution, one immediately obtains the value of t where intersection occurs:

$$t = \frac{(\vec{r}_c - \vec{r}_0) \cdot \vec{n}_\pi}{\vec{k}_0 \cdot \vec{n}_\pi} \tag{4}$$

and from Eq. 2, the coordinates of the reflection point. The incidence angle α_π is derived from $\sin\alpha_\pi = \underline{k}_0 \cdot \underline{n}_\pi$ and, for a symmetric reflection, the direction of the reflected ray (Eq. A.2) is $\underline{k}_1 = \underline{k}_0 - 2(\underline{k}_0 \cdot \underline{n}_\pi)\underline{n}_\pi$. The intersection point of the ray with the paraboloidal surface is computed in a similar manner, accounting for the variation of the normal $\underline{n}$ throughout the surface and the mirror imperfections (see Appendix A). For the beam expander, reflection is computed from the normal to the crystalline planes $\underline{n}_{\pi'}$, and accounting for the dispersivity properties of asymmetric crystals:[18]

$$\vec{k}_2 - \vec{k}_1 = \vec{n}_{\pi'} \frac{\lambda}{d_{220}}. \tag{5}$$

4. MIRROR PERFORMANCE SIMULATIONS VS. TESTS AT PANTER

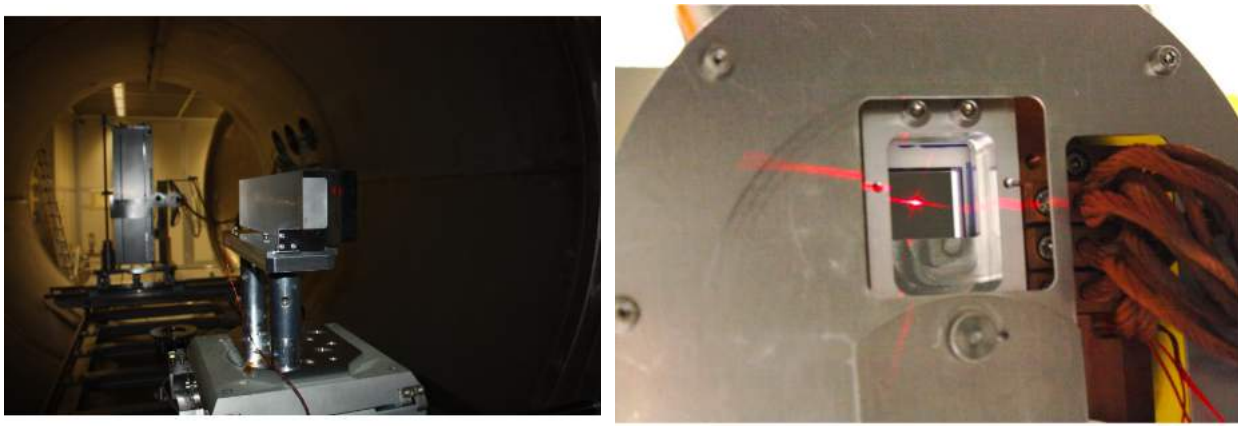

Figure 9: the BEaTriX mirror at PANTER. Left: before coating, in the PANTER vacuum tank. The detector stage, housing the TRoPIC and the PIXI detectors, is visible in the background. Right: the alignment laser, sharply focused on the TRoPIC sensor.

A fundamental step in the BEaTriX mirror finishing has been represented by full-illumination X-ray tests at PANTER, pre- and post-coating, aiming at confirming the predictions from metrology and at accepting the mirror for installation in the BEaTriX facility. The mirror was mounted in the PANTER vacuum tank and pre-aligned with the laser beam (Figure 9). In a first stage, the mirror has been probed with the low-diverging beam propagating freely from the PANTER source (127 m away). Due to the very good optical quality of the mirror, the coma aberration due to the source finite distance is the dominant term (Figure 6), contributing to the total HEW with 4.5 arcsec.

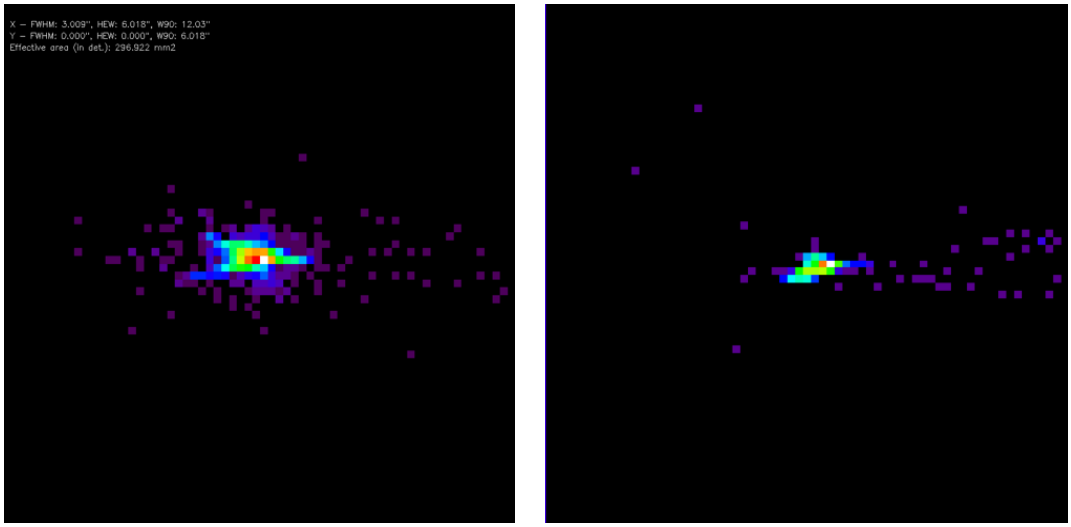

Figure 10: the best focus of the uncoated BEaTriX mirror at 1.49 keV with TRoPIC spatial resolution (pixel size: 3.3 arcsec) and in diverging *beam setup. Left: from simulation, HEW = 5 arcsec. Right: measured with TRoPIC, HEW = 4.8 arcsec. A 4.5 arcsec contribution comes from the divergence of the incoming beam.*

Nevertheless, the focus appeared very sharp and comparable in size with the detector pixels (TRoPIC: 75 μm, PIXI: 20 μm). The tests performed with the diverging beam at 1.49 keV revealed excellent agreement between predictions and experimental results (Figure 10). The HEW measurement in the best focus - which is, in diverging setup, shifted 200 mm downstream - returned 4.8 ± 1.6 arcsec at 1.49 keV and an absolute focal length of 4956 mm from the mirror center, as per our expectations.

As mentioned in Sect. 3.2, the 1.49 keV X-ray beam at PANTER can be made parallel using a zone plate.[26] The parallel beam setup removed completely the coma aberration from the setup and so yielded even better results (Figure 11, center). Even with some uncertainty due to the background noise in the PIXI camera and the finite pixel size (0.9 arcsec), **the measured *HEW is close to 3 arcsec*** and perfectly aligned to the simulation (Figure 11, left). The measured

value also includes the contribution of the source size at PANTER (approx. 0.5 arcsec), so the intrinsic HEW of the mirror itself is probably smaller.

The mirror performances did not relevantly vary from before to after coating deposition at DTU in between the two campaigns at PANTER (Figure 11, right). After the PANTER tests, the coated surface was also re-measured with the CCI, and no roughness increase was observed following the coating process, witnessing the excellent quality of the Pt+Cr reflective layer. After coating, the mirror has become reflective at 4.51 keV, an energy where the zone plate does not work; hence, we have no direct measurement in parallel beam at the X-ray energy of operation. Measurements performed with the diverging beam at this energy, however, returned a HEW near 6.5 arcsec. The 1.5 arcsec increase is probably due to the contribution of mirror areas *outside* the region that will reflect toward the asymmetric crystal and that are known to have a much worse roughness. Moreover, those areas would not contaminate the expanded beam, because a mirror slit will prevent them from being illuminated by the microfocus source.

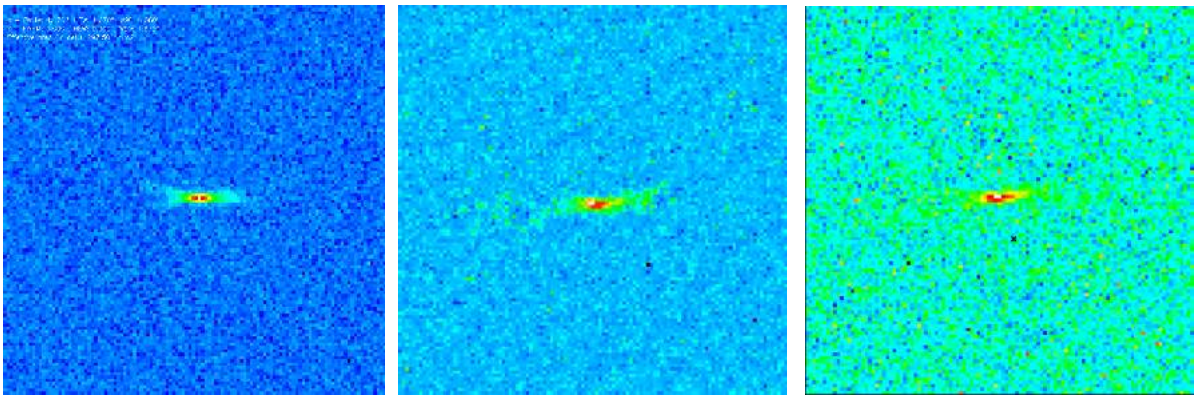

Figure 11: the best focus of the BEaTriX mirror at 1.49 keV with PIXI spatial resolution (pixel size: 0.9 arcsec) and in parallel *beam setup. Left: from simulation, HEW = 2.7 arcsec. Center: uncoated mirror, measured with PIXI, HEW = 3.1 arcsec. Right: after coating, measured with PIXI, HEW = 2.8 arcsec.*

5. SIMULATIONS OF THE EXPANDED BEAM COLLIMATION AND UNIFORMITY

5.1. The ideal BEaTriX system

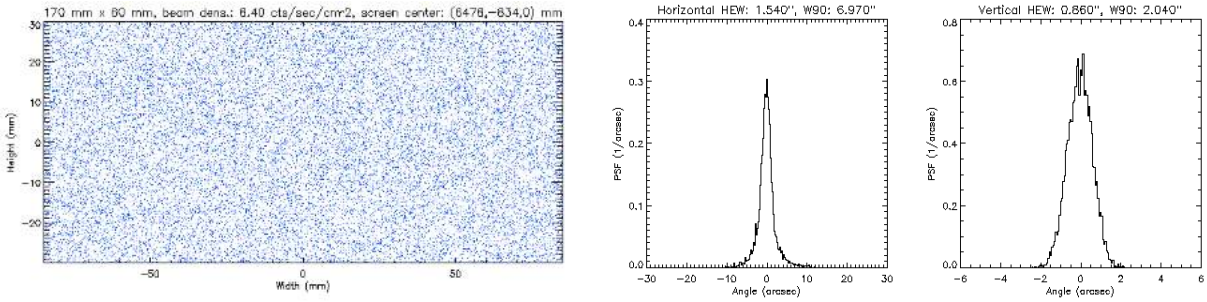

Figure 12: full simulation of the BEaTriX expanded beam for a perfect paraboloidal mirror and perfect alignment. Left: beam uniformity and dimensions. Right: due to the source size and the spectral bandpass through the monochromator, an ideal optical chain returns a beam with a HEW = 0.9 arcsec in vertical and 1.5 arcsec in horizontal.

Running the full BEaTriX simulation program (Figure 8) with a flawless paraboloidal mirror and all the components perfectly aligned, the result is shown in Figure 12. The viewgraphs correspond to the best achievable results in the BEaTriX facility: a 17 cm × 6 cm uniform beam, with a flux density of 8.4 counts/s/cm^2. The vertical divergence, almost solely due to the dimensions of the microfocus X-ray source, is near 0.9 arcsec HEW and will represent the divergence in the incidence plane of the MMs to be tested, therefore it is the most important parameter for probing their focusing properties. The horizontal divergence (HEW = 1.5 arcsec) is determined by the source size *and* by the spectral bandpass out of the monochromators.[19] This divergence component is the most sensitive to mirror imperfections, because a poor collimation by the paraboloid would increment the angle-energy combinations fulfilling the Bragg law in the symmetric crystals. This would in turn increase the angular dispersion in the asymmetric crystal.

5.2. Accounting for mirror imperfections and metrology

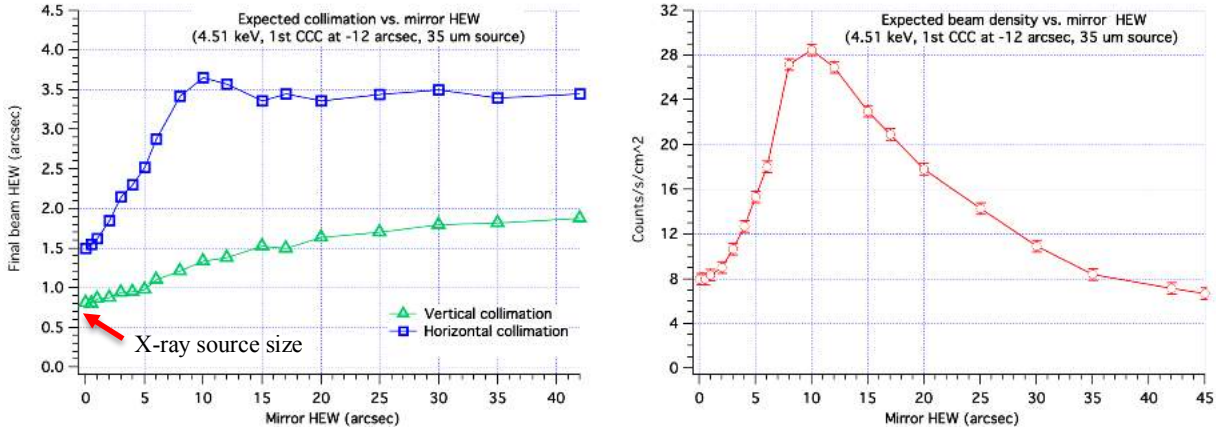

Figure 13: simulated impact of imperfections of the BEaTriX collimating mirror on (left) the vertical and horizontal collimation and (right) the beam flux. The vertical collimation is mostly affected by the size of the X-ray source, while the horizontal collimation is more severely degraded as the mirror quality gets worse. The beam intensity exhibits a peak where the mirror HEW starts to exceed the monochromators' rocking curve widths. However, the price for higher intensity can be a nonuniform beam.

Performing an extensive set of simulations with the BEaTriX simulation code and modeling variable levels of optical finishing,[19] this time up to a 45 arcsec HEW for the mirror (which was not far, indeed, from the initial quality of the pre-formed mirror),[15] we obtain the trends in Figure 13. The vertical collimation, essentially depending on the source size, is the least sensitive to the mirror quality. In contrast, the horizontal divergence degrades in proportion to the mirror quality, up to a plateau from 10 arcsec onwards. The saturation is explained by the rejection of rays impinging on the symmetric crystals with angles out of the narrow rocking curves of Si (220) diffraction order. At these angles, indeed, the energy shift needed to fulfill the Bragg condition would be larger than the natural width of the Ti-Kα1 line. This also justifies the intensity drop beyond 10 arcsec (Figure 13, right). The current situation of BEaTriX with a paraboloidal mirror having a measured HEW in the 3 - 4.5 arcsec range locates *the vertical divergence at 1 arcsec HEW and the horizontal one at 2.2 arcsec HEW*, perfectly suitable for testing SPO MMs. We also note that, thanks to the filtering effect of monochromators, a degradation by *1 arcsec* in the paraboloidal mirror will result in just a *0.2 arcsec* worsening of the expanded beam.

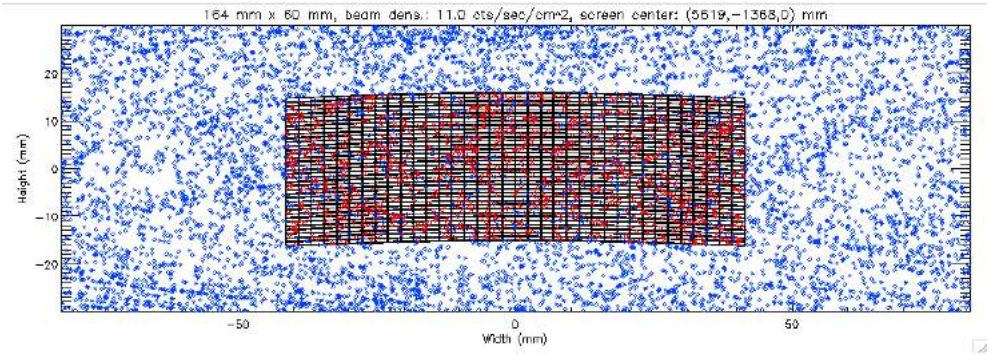

Figure 14: expanded beam dimensions and uniformity expected from the current status of the collimating mirror in BEaTriX. Also simulated is the incidence on a single XOU of ATHENA (one of the row No.8 in the current ATHENA design). Red markers represent the rays that have struck on a reflective surface of the SPO mirror module.

It is also possible to directly forecast the properties of the expanded beam from the current paraboloid metrology dataset (Sect. 3.1). The result is shown in Figure 14, where we have simulated the insertion of a mirror module in the expanded beam, and in Figure 15. The collimation and the intensity of the expanded beam match very well the values obtained from the expectation trend shown in Figure 13. Even if the beam uniformity is somehow altered by the mirror imperfections, the nonuniformity will not compromise the optical module PSF measurement. Neither will it hamper the effective area measurement, if the focused intensity is properly normalized to the beam intensity that will actually enter the mirror aperture (Sect. 5.3).

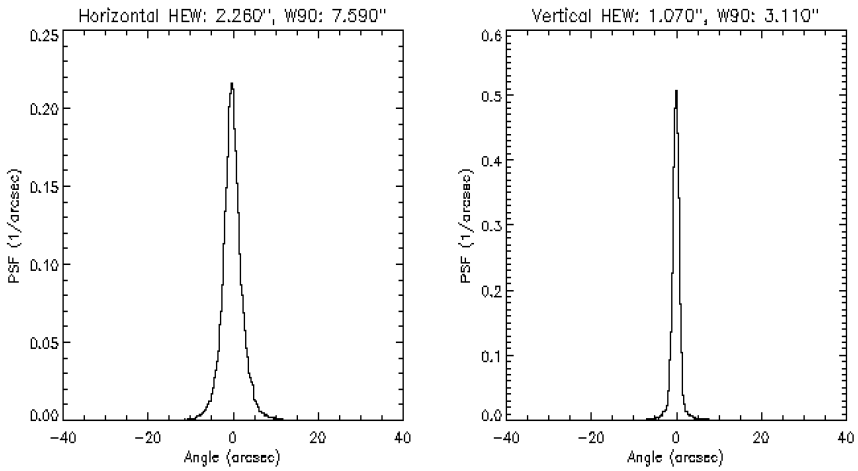

Figure 15: expected collimation in the expanded beam of BEaTriX, from the final status of the paraboloidal mirror.

5.3. Simulating the incidence on an SPO mirror module

An alternative method to assess the properties of the BEaTriX beam consists in prolonging the ray-tracing to the mirror module chamber (Figure 3) and simulating the reflection process in the complex structure of a silicon pore optic, as already sketched in Figure 14. For simplicity, but without loss of significance, we have taken an X-ray Optical Unit (XOU, half a MM) of the row No. 8 in the current mirror module assembly in the ATHENA design, assumed perfect (HEW = 0 arcsec) and 100% reflective. If the mirror module is exactly aligned on-axis, rays in the expanded beam can either be stopped on a membrane/rib wall, or be reflected. A small fraction of the reflected rays misses the second reflection and is baffled by the SPO structures, while all the others make the second reflection and reach the focus.

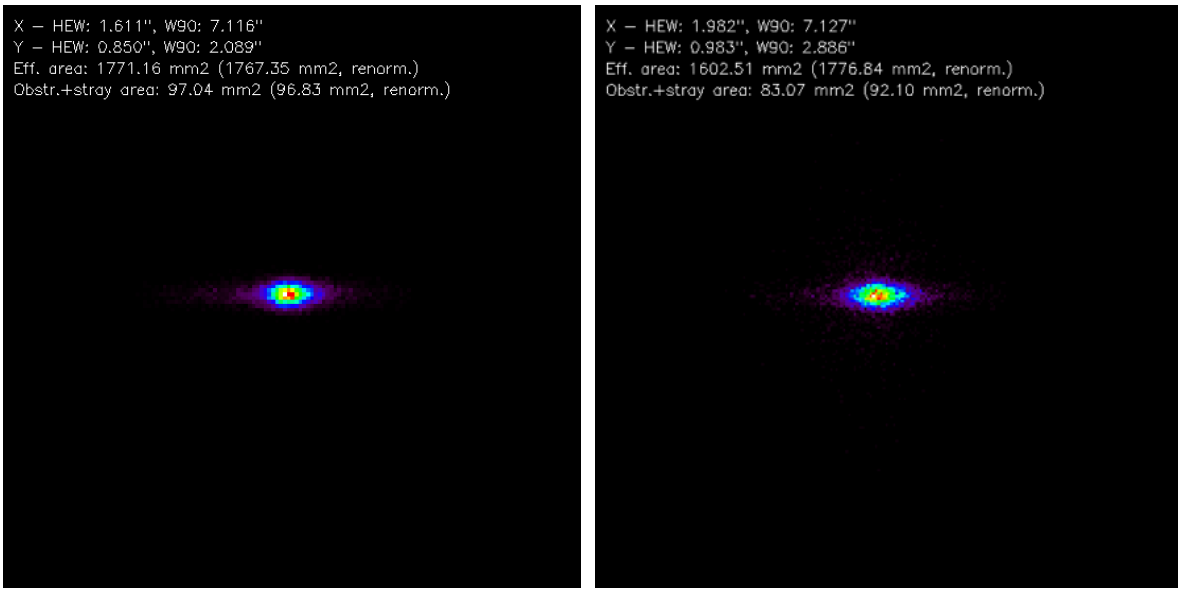

Figure 16: simulated focus of a perfect mirror module in the BEaTriX expanded beam. Left: in a perfect BEaTriX system. Right: with the current manufacturing status of the paraboloidal mirror. In both cases, the focus appears elongated horizontally due to the better beam collimation in the vertical plane, which is also the incidence plane of the MM to be tested. Residual mirror imperfections chiefly degrade the focus horizontally. The images have a 3 mm size.

Figure 16 shows what to expect in the focus of the MM, at the end of the long arm of BEaTriX. In an ideal system (Sect. 5.1), the focus has the shape of an ellipse with the axes equal to the vertical and horizontal HEW values reported in Figure 12. With the real paraboloid, the vertical size will be only slightly larger, while the horizontal size will be broader due to the increased divergence. In this case also, the focal spot dimensions correspond to the divergence values assessed from the angular deviations (Figure 15).

As for the effective area, the 17.67 cm^2 found with the "perfect" BEaTriX beam is exactly what one would find analytically.[24] Even though nonuniformities in the "real" expanded beam can alter this measurement, renormalizing the focus brightness to the intensity impinging onto the mirror module aperture will allow us retrieving the correct effective area value to within a few percent accuracy (17.76 cm^2).

6. DETECTING SOURCE MISALIGNMENTS VIA WAVEFRONT SENSING

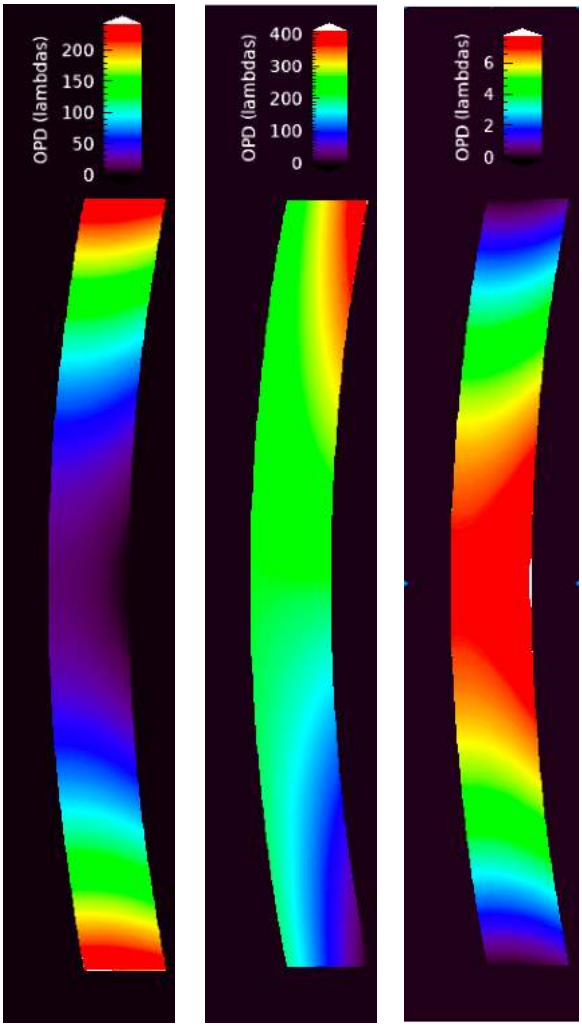

Figure 17: simulated wavefront out of the BEaTriX mirror due to misalignments by 1 mm (left) along the radius; (center) in vertical direction; (right) along the rays. The color scales express the optical path difference in units of lambda.

Just like manufacturing the paraboloidal mirror is a fundamental step, a precise alignment of the mirror focus to the source is also necessary for ensuring the expanded beam collimation. We have already discussed this problem in a previous contribution[19] and determined that accurate alignment in X-rays can be achieved using a wavefront sensor (WFS). Therefore, we are planning to use a WFS in collaboration with Brookhaven National Labs, ENSTA-Paris and Imagine Optic to diagnose the collimated beam out of the BEaTriX mirror. From the wavefront deformation, the mirror-to-source misalignments can be measured and corrected by means of the vacuum motors.

The wavefront deformations expected from the three possible source displacements can be modeled using one of the functionalities implemented in the full BEaTriX simulation program (Sect. 3.3), but the ray statistics requires an unacceptably long time to perform a systematic investigation. We would rather use an approach based on physical optics, reversing the program used to propagate the wavefront to the focus (Figure 6, left). In all the cases considered, the phase shifts used to back-propagate the beam from the source to the detection plane are the projected differences in the radial coordinate between the nominal paraboloid and the paraboloid that would exactly focus the beam at the current location of the source. Three examples, shown in Figure 17, illustrate the expected wavefront shapes that would be detected by the wavefront sensor near the mirror, in the presence of a misaligned source, along three independent directions in space (tilt terms were mostly removed). The wavefront shapes can be analyzed in terms of Zernike polynomials or beamlet displacements out of a Hartmann plate. As already pointed out,[19] source displacements in the incidence plane mainly defocus the beam, while displacements in the sagittal plane twist the wavefront, introducing coma and astigmatism terms. Displacements along the rays exhibit an effect totally similar to the one of displacements along the radius, but the wavefront is much less sensitive to this kind of displacement. A systematic analysis of the wavefront distortion caused by source misalignments will give us confidence with this tool before proceeding to the forthcoming alignment of the paraboloidal mirror in BEaTriX.

7. FINAL REMARKS

The ongoing assembly of the BEaTriX X-ray facility at INAF-Brera and the alignment of the optical components is being assisted by a set of optical simulations. To this aim, we have explored a variety of approaches, based on both geometric and physical optics. Some simulations were addressed at predicting the optical quality of the paraboloidal mirror from the available metrology data, in very good agreement with experiments at PANTER. Other software tools

have been used to predict the effect of the collimating mirror on the divergence, the uniformity, and the intensity of the expanded beam at the different stages of the mirror finishing. As we approach the alignment of the mirror in the 4.51 keV beamline of BEaTriX, wavefront distortion simulations are being suited to gain confidence with the precise alignment process. Future work will extend the simulations to the 1.49 keV beamline of BEaTriX.

APPENDIX A. IN- AND OUT-OF-PLANE SCATTERING IN RAY-TRACING

In a mirror surface described by the rotation of the profile $r(z)$ about the z-axis, the unit normal vector at the ray impact point, located by the cylindrical coordinates (φ_0, z_0), is given by

$$\vec{n} = (-\cos\alpha_0 \cos\varphi_0\,, -\cos\alpha_0 \sin\varphi_0\,, \sin\alpha_0) \tag{A.1}$$

where $\alpha_0 = \tan^{-1}(r'(z_0))$ is the incidence angle for an on-axis ray. The usual formula providing the reflected ray direction, $\underline{k}_1$, as a function of the incident direction $\underline{k}_0$ and the local normal vector:

$$\vec{k}_1 = \vec{k}_0 - 2(\vec{k}_0 \cdot \vec{n})\vec{n} \tag{A.2}$$

(where "·" denotes a scalar product of vectors), returns a final ray direction that is correctly normalized to 1,

$$|\vec{k}_1|^2 = (\vec{k}_0 \cdot \vec{k}_0) - 4(\vec{k}_0 \cdot \vec{n})^2 + 4(\vec{k}_0 \cdot \vec{n})^2 |\vec{n}|^2 = |\vec{k}_0|^2 = 1, \tag{A.3}$$

and forming with the initial ray direction an angle α_{01} such that:

$$\vec{k}_1 \cdot \vec{k}_0 = 1 - 2(\vec{k}_0 \cdot \vec{n})(\vec{k}_1 \cdot \vec{n}). \tag{A.4}$$

In specular reflection, the angle between $\underline{k}_1$ and $\underline{n}$ is the same as between $\underline{k}_0$ and $\underline{n}$, i.e., $\underline{k}_0 \cdot \underline{n} = \sin\alpha_0$, so we get

$$\vec{k}_1 \cdot \vec{k}_0 = 1 - 2\sin^2\alpha_0 = \cos 2\alpha_0; \tag{A.5}$$

which correctly implies that the angle between $\underline{k}_1$ and $\underline{k}_0$ is $\alpha_{01} = 2\alpha_0$. If the mirror is imperfect, in order to preserve the validity of Eq. (A.2), we will have to alter the local normal vector (A.1) to account for both ray deviations: in the incidence plane, and orthogonal to the incidence plane.

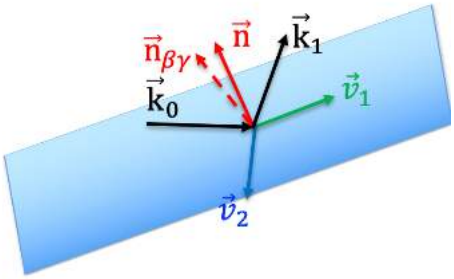

Figure A.1: the reference frame for a proper treatment of in-plane and out-of-plane ray deflections.

As for in-plane scattering, we want $\underline{k}_1$ to form a larger angle with $\underline{k}_0$, i.e., $2\alpha_0+2\beta$. We therefore rotate the normal vector by an angle β in the incidence plane. For the new normal vector $\underline{n}_\beta$ to lie in the ($\underline{k}_0$, $\underline{n}$) plane, it has to be an appropriate linear combination of them. More exactly, we replace $\underline{n}$ in Eq. (A.2) with

$$\vec{n}_\beta = \vec{n}\cos\beta + \vec{v}_1 \sin\beta. \tag{A.6}$$

The first term is the component coming from the original normal $\underline{n}$, while the second one, proportional to

$$\vec{v}_1 = \frac{\vec{k}_0 - (\vec{k}_0 \cdot \vec{n})\vec{n}}{\sqrt{1 - (\vec{k}_0 \cdot \vec{n})^2}} \tag{A.7}$$

is the $\underline{k}_0$ component orthogonal to $\underline{n}$ (i.e., $\underline{k}_0$ *minus* its component parallel to $\underline{n}$). We can immediately see that the two components are mutually orthogonal and normalized to 1. The new normal, $\underline{n}_\beta$, is normalized to 1 also:

$$|\vec{n}_\beta|^2 = |\vec{n}|^2\cos^2\beta + 2\frac{(\vec{k}_0 \cdot \vec{n}) - (\vec{k}_0 \cdot \vec{n})}{\sqrt{1 - (\vec{k}_0 \cdot \vec{n})^2}}\cos\beta\sin\beta + |\vec{v}_1|^2\sin^2\beta = \cos^2\beta + \sin^2\beta = 1, \tag{A.8}$$

and, similarly to Eq. (A.5), the angle between $\underline{k}_0$ and $\underline{k}_1$ takes on the expected value: using Eq. (A.2) with $\underline{n}_\beta$, we get

$$\vec{k}_0 \cdot \vec{k}_1 = 1 - 2\left(\vec{k}_0 \cdot \vec{n}_\beta\right)^2 = 1 - 2\left[\left(\vec{k}_0 \cdot \vec{n}\right)\cos\beta + \left(\vec{k}_0 \cdot \vec{v}_1\right)\sin\beta\right]^2 =$$
$$= 1 - 2[\sin\alpha_0 \cos\beta + \cos\alpha_0 \sin\beta]^2 = 1 - 2\sin^2(\alpha_0 + \beta) = \cos(2\alpha_0 + 2\beta). \quad \text{(A.9)}$$

A deviation in the orthogonal direction by an angle γ, due to out-of-plane scattering, can be modeled adding a third vector component:

$$\vec{v}_2 = \vec{n} \times \vec{v}_1 = \frac{\vec{n} \times \vec{k}_0}{\sqrt{1 - \left(\vec{k}_0 \cdot \vec{n}\right)^2}} \quad \text{(A.10)}$$

("×" means cross vector product), which is also normalized and, clearly, orthogonal to the incidence plane. The perturbed normal vector is therefore represented by an extension of Eq. (A.6) to spherical coordinates:

$$\vec{n}_{\beta\gamma} = \vec{n}\cos\beta\cos\gamma + \vec{v}_1 \sin\beta\cos\gamma + \vec{v}_2 \sin\gamma. \quad \text{(A.11)}$$

Using Eq. (A.11), the reflection direction from the imperfect mirror is obtained generalizing Eq. (A.2):

$$\vec{k}_1 = \vec{k}_0 - 2\left(\vec{k}_0 \cdot \vec{n}_{\beta\gamma}\right)\vec{n}_{\beta\gamma}. \quad \text{(A.12)}$$

We note that, in grazing incidence, the effect of the out-of-plane deflection is automatically damped[23] by a factor of $\tan\alpha_0$. The angle γ can therefore be computed as if the scattering occurred in the tangential plane, just like β, without the need to reduce its amplitude by a factor of $\tan\alpha_0$.

ACKNOWLEDGMENTS

The BEaTriX project is financed by ESA (contract #4000123152/18/NL/BW), AHEAD (grants #654215 and #871158), ASI (grant #2019-27-HH.0) and INAF funds. We thank Philippe Zeitoun (ENSTA-Paris), Ombeline De La Rochefoucauld (Imagine Optic), and Mourad Idir (Brookhaven National Labs) for the interest and the kind collaboration in the project.

REFERENCES

[1]. Bradshaw, M., Burwitz, V., Hartner, G., Langmeier, A., Vacanti, G., et al., "Testing ATHENA optics: a new measurement standard at the PANTER x-ray test facility," Proc. of SPIE 11852, 1185223 (2021)
[2]. Bavdaz, M., Wille, E., Ayre, M., Ferreira, I., Shortt, B., et al., "The Athena x-ray optics development and accommodation," Proc. SPIE 11852, 1185220 (2021)
[3]. Collon, M. J., Babic, L., Barrière, N. M., Bayerle, A., Castiglione, L., et al., "X-ray mirror development and production for the Athena telescope," Proc. SPIE 11852, 118521Z (2021)
[4]. Krumrey, M., Muller, P. et al., "New X-ray parallel beam facility XPBF 2.0 for the characterization of the silicon pore optics," Proc. SPIE 9905, 99055N (2016)
[5]. Vacanti, G., Barrière, N. M., Collon, M.J., Hauser, E., et al., "X-ray testing of Silicon Pore Optics," Proc. SPIE 11119, 1111901 (2019)
[6]. Burwitz, V., Bavdaz, M, Wille, E., Collon, M., et al., "X-ray testing at PANTER of optics for the ATHENA and Arcus Missions," Proc. SPIE 11180, 1118024 (2019)
[7]. Spiga, D., Pareschi, G., Pelliciari, C., et al., "Functional tests of modular elements of segmented optics for x-ray telescopes via an expanded beam facility," Proc. SPIE 8443, 84435F (2012)
[8]. Spiga, D., Pelliciari, C., Bonnini, E., et al., "An expanded x-ray beam facility (BEaTriX) to test the modular elements of the ATHENA optics," Proc. SPIE 9144, 91445I (2014)
[9]. Pelliciari, C., Spiga, D., Bonnini, E., et al., "BEaTriX, expanded soft x-ray beam facility for test of focusing optics, an update," Proc. SPIE 9603, 96031P (2015)
[10]. Spiga, D., Pelliciari, C., Salmaso, B., et al. "Design and advancement status of the Beam Expander Testing X-ray facility (BEaTriX)," Proc. SPIE 9963, 996304 (2016)

[11]. Salmaso, B., Spiga, D., Basso. S., Ghigo, M., Giro, E., Pareschi, G., Tagliaferri, G., Vecchi, G., et al., "Progress in the realization of the beam expander testing x-ray facility (BEaTriX) for testing ATHENA's SPO modules," Proc. SPIE 10699, 1069931 (2018)
[12]. Salmaso, B., Spiga, D., Basso. S., Ghigo, M., Giro, E., Pareschi, G., Tagliaferri, G., Vecchi, et al., "BEaTriX (Beam Expander Testing X-ray facility) for testing ATHENA's SPO modules: advancement status," Proc. SPIE 11180, 1118026 (2019)
[13]. Valsecchi, G., Bianucci, G., Marioni, F., Vernani, D., Zocchi, F., Korhonen, T., Pasanen, M., Pareschi, G., Ferreira, F., Bavdaz, M., Wille, E., Doyle, D., "Facility for alignment, assembly, and integration of the SPO mirror modules onto the ATHENA telescope," Proc. SPIE 11822 (2021)
[14]. Moretti, A., Spiga, D., Sironi, G., Pareschi, G., Basso, S. Tagliaferri, G., Valsecchi, G., Zocchi, F., Vernani, D., Marioni, F., Tordi, M., De Lorenzi, S., Parodi, G., Amisano, F., Corradi, P., Ottolini, M., Ferreira, I., Bavdaz, M., Parissenti, G., La Palombara, N., Uslenghi, M., Civitani, M, Ghigo, M. "The VERT-X calibration facility: development of the most critical parts," Proc. SPIE 11822 (2021)
[15]. Salmaso, B., Basso, S., Cotroneo, V., Ghigo, M., Pareschi, G., Redaelli, E., Sironi, G., Spiga, D., Tagliaferri, G., Vecchi, G., Fiorini, M., Incorvaia, S., Uslenghi, M., Paoletti, L., Ferrari, C., Zappettini, A., Lolli, R., Sanchez del Rio, M., Burwitz, V., Christensen, F., Della Monica Ferreira, D., Gellert, N., Massahi, S., Bavdaz, M., Ferreira, I., "Building the BEaTriX facility for the ATHENA mirror modules X-ray testing," Proc. SPIE 11822 (2021)
[16]. Vecchi, G., Salmaso, B., Basso, S., Sironi, G., et al., "BEaTriX, the Beam Expander Testing X-ray facility for testing ATHENA's SPO modules: the collimating mirror," Proc. SPIE 11119, 111191J (2019)
[17]. Christensen, F., Hornstrup, A., Frederiksen, P., et al., "Expanded beam x-ray optics calibration facility at the Daresbury Synchrotron," Proc. SPIE 2011, 540 (1994)
[18]. Sanchez del Rio, M., Cerrina, F., "Asymmetrically cut crystals for synchrotron radiation monochromators", Review of Scientific Instruments 63, 936 (1992)
[19]. Spiga, D., Salmaso, B., Bavdaz, M., Pelliciari, C., Basso, S., Burwitz, V., Ferreira, I., Ghigo, M., Giro, E., Pareschi, G., Sanchez del Rio, M., et al., "Optical simulations for the laboratory-based, expanded and collimated X-ray beam facility BEaTriX," Proc. SPIE 11110, 111100E (2019)
[20]. Ferrari, C., Beretta, S., Salmaso, B., Pareschi, G., Tagliaferri, G., et al., "Characterization of ADP crystals for soft x-ray optics of the Beam Expander Testing X-ray facility (BEaTriX)," Journal of Applied Crystallography 52, 599-604 (2019)
[21]. Vecchi, G., Cotroneo, V., Ghigo, M., Basso, S., Salmaso, B., Sironi, G., Spiga, D., Conconi, P., Pareschi, G., Tagliaferri, G., Burwitz, V., Hartner, G., Müller, T., Rukdee, S., Schmidt, T., Christensen, F., Della Monica Ferreira, D., Gellert, N., Massahi, S., Bavdaz, M., Ferreira, I., "Manufacturing and testing of the X-ray collimating mirror for the BEaTriX facility", Proc. SPIE 11822 (2021)
[22]. Sironi, G., Citterio, O., Pareschi, G., Negri, B., Ritucci, A., Subranni, R., Orlandi, A., Borghi, G., Stroebel, M., Arnold, J., Widemann, R., et al., "MPR: innovative 3D free-form optics profilometer," Proc. SPIE 8147, 814718 (2011)
[23]. Spiga, D., Raimondi, L., "X-ray optical systems: from metrology to Point Spread Function," Proc. SPIE 9209, 92090E (2014)
[24]. Spiga, D., Della Monica Ferreira, D., Shortt, B., Bavdaz, M., Bergback Knudsen, E., Bianucci, G., Christensen, F., Civitani, M., Collon, M., Conconi, P., Fransen, S., et al., "Optical simulations for design, alignment, and performance prediction of silicon pore optics for the ATHENA x-ray telescope," Proc. SPIE 10399, 103990H (2017)
[25]. Spiga, D., Moretti, A., Pareschi, G., Sironi, G., Tagliaferri, G., Bavdaz, M., Ferreira, I., Valsecchi, G., Marioni, F., Zocchi, F., "Optical simulations for the Wolter-I collimator in the VERT-X calibration facility," Proc. SPIE 11822 (2021)
[26]. B. Menz, H. Brauninger, V. Burwitz et al., "Studying ATHENA optics with divergent and collimated x-ray beams," Proc. SPIE 9144, 91445J (2014)